Atmospheric controls of the heat balance of Zongo Glacier (16°S, Bolivia)

Jean-Emmanuel Sicart, Patrick Wagnon, Pierre Ribstein

Atmospheric controls of the heat balance of Zongo Glacier (16°S, Bolivia)

Jean Emmanuel Sicart
Great Ice Research Unit, l'Institut de Recherche Pour le Développement, Université Montpellier II, Montpellier, France

Patrick Wagnon
Great Ice Research Unit, l'Institut de Recherche Pour le Développement, Laboratoire de Glaciologie et Geophysique de l'Environnement, Saint Martin d'Hères, France

Pierre Ribstein
UMR Sisyphe, Université Pierre et Marie Curie, Paris, France

Received 22 December 2004; revised 8 March 2005; accepted 23 March 2005; published 21 June 2005.

[1] Tropical glaciology includes investigation of climate variability in poorly documented regions of large surface-atmosphere energy exchanges. This study examines the surface energy fluxes of the Bolivian Zongo Glacier (16°S, 68°W, 6000–4900 m asl) in order to identify the atmospheric variables that control melting. Measurements from 1998 to 2000 taken from two meteorological stations in the ablation area are analyzed. During the progressive development of the wet season from September to January, melting energy was high: Solar irradiance was close to its summer solstice peak, clouds were sporadic, and albedo was low. During the core of the wet season from January to April the magnitudes of the net short-wave (+) and net long-wave (−) radiation fluxes were reduced by frequent clouds and snowfalls so that melting energy was moderate. In the dry season from May to August, melting energy was small because of the energy losses essentially in long-wave radiation but also in sublimation. The turbulent sensible heat flux to the ice (+) generally offsets the energy loss in latent heat (−), except in the dry season, when sublimation prevailed because of strong wind and dry air. Solar radiation was the main source of energy, but the seasonal changes of the melting energy were driven by long-wave radiation. In particular, clouds sharply increased the emittance of the thin high-altitude atmosphere. Closely linked to clouds and humidity, the main seasonal variables of low-latitude climates, long-wave radiation is a key variable in the energy balance of tropical glaciers.

Citation: Sicart, J. E., P. Wagnon, and P. Ribstein (2005), Atmospheric controls of the heat balance of Zongo Glacier (16°S, Bolivia), *J. Geophys. Res.*, *110*, D12106, doi:10.1029/2004JD005732.

1. Introduction

[2] Recent studies have emphasized the role of low-latitude regions in global climate changes [e.g., *Seltzer*, 2001; *Visser et al.*, 2003]. Monitoring tropical glaciers makes it possible to investigate climatic variability on annual to centennial timescales in poorly documented remote regions. Observations have demonstrated a general glacial recession throughout the 20th century in the Andes [e.g., *Hastenrath and Ames*, 1995; *Kaser*, 1999; *Francou et al.*, 2000; *Ramirez et al.*, 2001], Africa [e.g., *Kaser and Noggler*, 1991; *Mölg et al.*, 2003] and Irian Jaya [*Peterson and Peterson*, 1994]. *Thompson* [2000] attributed the tropical glacial recession to a warming of the troposphere. However, *Gaffen et al.* [2000] reported a cooling of the tropical low troposphere after 1979, which contrasts with an acceleration of the recession of the Central Andean glaciers [*Ramirez et al.*, 2001]. *Vuille et al.* [2003] reported a humidity increase over the last three decades in the atmosphere south of 11°S. A humidity increase can enhance glacier ablation through condensation heat release, an increase in sky long-wave radiation, or a reduction in ice sublimation. Satellites revealed a strengthening of the tropical general circulation in the 1990s, leading to an increase (decrease) of cloud cover at the equator (in the subtropical latitudes) [*Chen et al.*, 2002; *Wielicki et al.*, 2002]. However, glaciers have been observed to shrink in all tropical regions, from the inner to the outer tropics [*Kaser*, 2001; *Francou et al.*, 2003, 2004].

[3] The climate controls the mass balance of glaciers through the energy and mass fluxes at the ice or snow interface. Energy measurements are scarce on tropical glaciers, and they are generally short term [e.g., *Platt*, 1966; *Hastenrath*, 1978; *Hardy et al.*, 1998; *Mölg et al.*,

0148-0227/05/2004JD005732

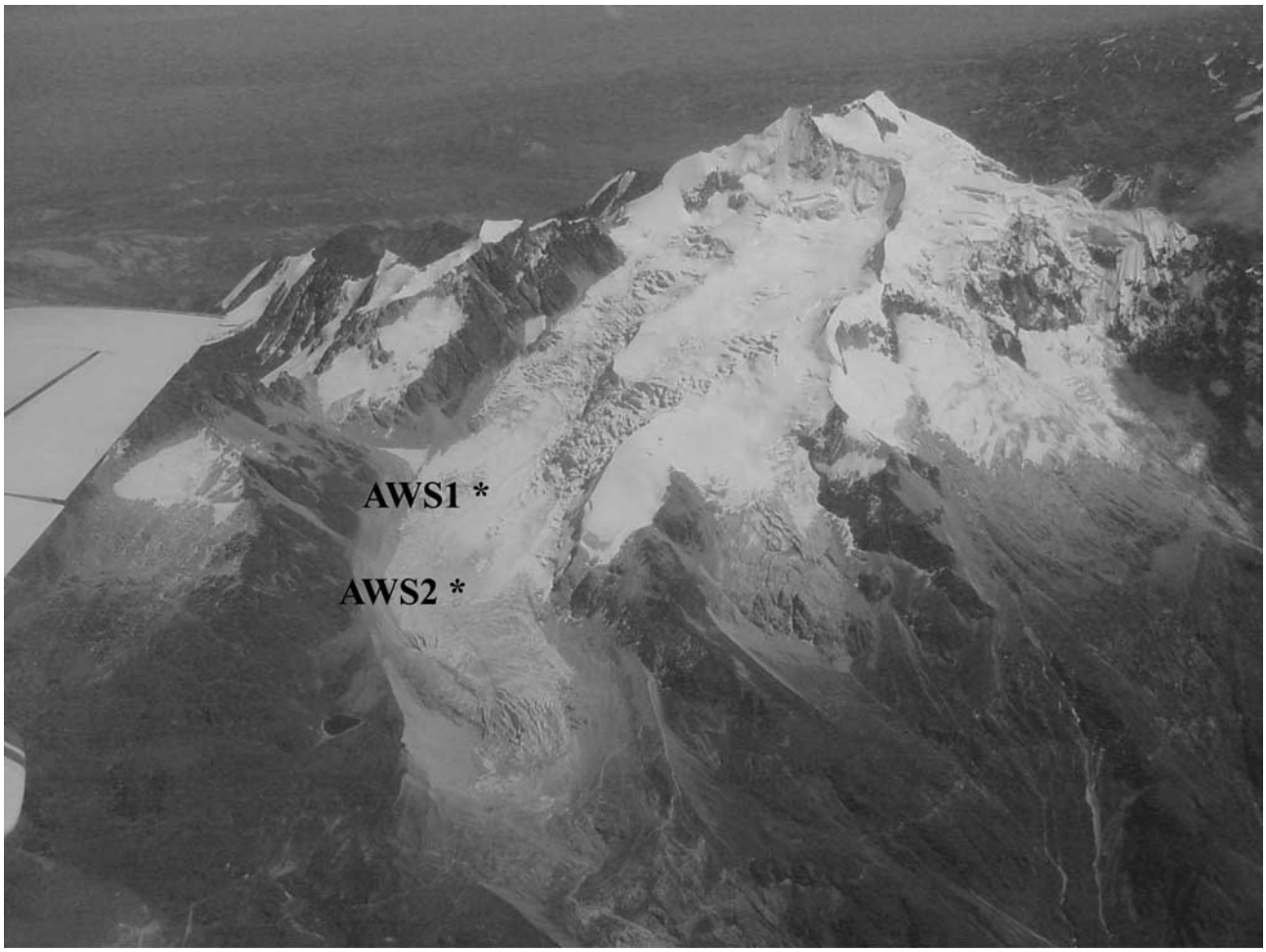

Figure 1. Aerial photograph of the Zongo Glacier (4 August 2000, B. Pouyaud) showing the locations of AWS1 (5150 m asl) and AWS2 (5060 m asl).

2003]. The French institute IRD has been conducting an extensive meteoglaciological program on the Zongo Glacier, Cordillera Real, Bolivia (16°S, 68°W) since 1991 [*Ribstein et al.*, 1995]. The Zongo Glacier is situated in the outer tropics, characterized by humid tropical conditions during the wet season (austral summer) and by subtropical conditions during the dry season (austral winter). In the outer tropics, the Peruvian and the Bolivian glaciers compose 71 and 20% of the total surface area of the tropical glaciers, respectively [*Kaser et al.*, 1996].

[4] This study analyzed the energy fluxes at the surface of the Zongo Glacier. The objective was to improve the understanding of the climate forcing on tropical glaciers. Measurements taken from two meteorological stations between 1998 and 2000 close to the equilibrium line and in the ablation area were analyzed. *Wagnon et al.* [1999] discussed the turbulent fluxes of the dry season, and *Wagnon et al.* [2001] and *Sicart et al.* [2003] analyzed the annual cycle of the surface albedo. Here all the energy fluxes were analyzed and we focus on the radiation fluxes in the wet season, when the intensity and the interannual variability of the energy fluxes are maximal. New equipment for separate measurements of the short- and long-wave radiation fluxes improved the accuracy of these measurements compared to previous studies on the Zongo Glacier, and provided a proper analysis of the long-wave radiation fluxes.

2. Location and Measurement Program

[5] The Zongo Glacier is situated in the Huayna Potosi Massif (16°15′S, 68°10′W, Cordillera Real, Bolivia) on the western margin of the Amazon basin and on the eastern margin of the Altiplano catchment. This valley-type glacier is 3 km long and has a surface area of 2.4 km^2 (Figure 1). The glacier flows out from 6000 to 4900 m above sea level (asl). The equilibrium line altitude, estimated from stake measurements and snow pits, is roughly 5200 m asl for an equilibrated mass balance [*Sicart et al.*, 2005]. The Zongo Glacier is part of a 3.7-km^2 basin above the hydrometric station located at 4830 m asl. The site characteristics are presented in detail by *Francou et al.* [1995].

[6] Two Campbell Automatic Weather Stations (AWS), AWS1 at 5150 m asl and AWS2 at 5060 m asl, have been functioning on the glacier since March 1996 and July 1999, respectively (Figure 1 and Table 1). The weather stations are located close to the axis of the glacier, on flat areas: The

Table 1. List of Different Sensors at AWS1 and AWS2 With Their Specifications

Quantity[a]	AWS2 (5060 m asl) Sensor Type (Height[b])	AWS1[c] (5150 m asl) Sensor Type (Height[b])	Accuracy According to the Manufacturer
Air temperature,[d] °C	Vaisala HPM45C not aspirated (1 m)	Vaisala HPM45C aspirated (0.3 and 1.8 m)	±0.2°C
Relative humidity,[d] %	Vaisala HPM45C not aspirated (1 m)	Vaisala HPM45C aspirated (0.3 and 1.8 m)	±2% in [0–90%], ±3% in [90–100%]
Wind speed, m s^{-1}	Young 05103 (2.5 m)	Young 05103 (0.3 and 1.8 m)	±0.3 m s^{-1}
Wind direction, deg	Young 05103 (2.5 m)	Young 05103 (0.3 and 1.8 m)	±3 deg
Incident short-wave radiation, W m^{-2}	Kipp and Zonen CM3 (1 m) $0.305 < \lambda < 2.8$ μm	SKYE SKS1110 (1 m) $0.4 < \lambda < 1.1$ μm	CM3: ±10% for daily sums, sp1100: ±3%
Reflected short-wave radiation, W m^{-2}	Kipp and Zonen CM3 (1 m) $0.3 < \lambda < 2.8$ μm	SKYE SKS1110 (1 m) $0.4 < \lambda < 1.1$ μm	CM3: ±10% for daily sums, sp1100: ±3%
Incoming long-wave radiation, W m^{-2}	Kipp and Zonen CG3 (1 m) $5 < \lambda < 50$ μm	. . .	±10% for daily sums
Outgoing long-wave radiation, W m^{-2}	Kipp and Zonen CG3 (1 m) $5 < \lambda < 50$ μm	. . .	±10% for daily sums
Net all-wave radiation, W m^{-2}	Calculated from the four preceding quantities	REBS Q7 (1 m) $0.25 < \lambda < 60$ μm	±10% for daily sums
Accumulation/ablation, mm	. . .	Ultrasonic depth gauge Campbell UGD01 (1.5 m)	±1 cm

[a]Quantities are recorded as half-hourly means over 20-s time intervals except for wind direction and accumulation/ablation, which are instantaneous values every 30 min.
[b]Height changes are derived from the ultrasonic depth gauge measurements and the field visits every 15 days.
[c]AWS1 is described in its recent configuration (after March 2000), which slightly differs from the configuration by *Wagnon et al.* [1999, 2001].
[d]At AWS2 the Vaisala hygrothermometers are shielded from solar radiation and artificially ventilated. Artificial aspiration could not be maintained at AWS1 because of power supply requirements.

mean slopes at AWS1 and at AWS2 are 7° and 3°, respectively [*Sicart et al.*, 2001]. The stations are checked every 15–20 days all year round. Qualitative observations of the glacier surface and the meteorological conditions were conducted during the field visits and during extensive field trips lasting a few days. Direct daily sublimation measurements were taken during the field trips using "poor man's lysimeters:" translucent round plastic pails (165–395 cm^2), filled with snow/ice in order to reconstruct the natural surfaces, buried into the snow and regularly weighed, with an accuracy of ±1 g [*Wagnon et al.*, 1999].

[7] Vertical profiles of air temperature (Cu-Cst thermocouples, accuracy approximately ±0.3°C) were occasionally conducted at 5150 m asl (mean data every 5 min over 5-s time steps, continuous aspiration of 5 m s^{-1}). Seven sensors, shielded from radiation, were located at 2, 10, 20, 30, 40, 50, and 100 cm above the glacier surface. A liquid water–ice bath at 0°C was used as the temperature reference.

[8] Temperature and humidity measurements outside the thermal influence of the glacier were recorded by a weather station located 150 m below and 1 km from the glacier front.

3. Climatic Conditions

[9] The Huayna Potosi is in the outer tropics, characterized by a marked seasonality of precipitation and cloud cover with a single wet season in austral summer and a pronounced dry season in winter. The dry season (May to August) is produced by the northward displacement of the midtropospheric and upper-tropospheric westerlies, which prevent moisture influx from the east. Summer precipitation (September to April) is associated with intense solar heating of the Altiplano surface, leading to a destabilization of the boundary layer, inducing deep convection and moist air advection from the eastern interior of the continent [*Vuille et al.*, 2000]. The moist air is typically released in afternoon showers over the Altiplano [*Garreaud and Wallace*, 1997], but heavy nighttime snowfalls are also frequent on the glacier [*Sicart et al.*, 2002].

[10] The hydrological year is counted from the end of the dry season, 1 September. The annual precipitation is roughly 1 m w.e. The ultrasonic depth gauge measurements illustrate the accumulation and the ablation close to the equilibrium line (Figure 2). From September to December, periods of heavy melting (several centimeters of ice/snow per day) alternate with snowfalls that become increasingly frequent. Since melting and precipitation generally alternate on the same day, the daily height changes represent a net accumulation or a net ablation. The gradual buildup to the full wet season is observed in the Andes from Bolivia to Peru [*Schwerdtfeger*, 1976] and can be considered as a transition period. The wet season lasts roughly from January to April. On average, it snows 2 days out of 3, and the net daily accumulation is steady: around 20 mm of snow per day. In April, the change to the dry season is rather sudden. A few snowfall events may occur but the dry season is generally a period of moderate ablation until the end of August (Figure 2).

[11] The annual cycle of air humidity reflects the alternation of the wet and dry seasons (Figure 2). In contrast, the thermal seasonality is low; less than 10°C (Figure 2). On the glacier, the mean annual temperature is about −1°C at the equilibrium line. The limit elevation between snow and rain changes little throughout the year; it remains lower than 5050 m asl and only affects a small area of the glacier. In the wet season, the valley wind from the east or southeast prevails during the daytime (1000–1800 LT), whereas the downslope glacier wind, from the northwest, is observed at night (Figure 3). The glacier wind prevails most of the day in the dry season, except a few hours around 1400 LT (Figure 3).

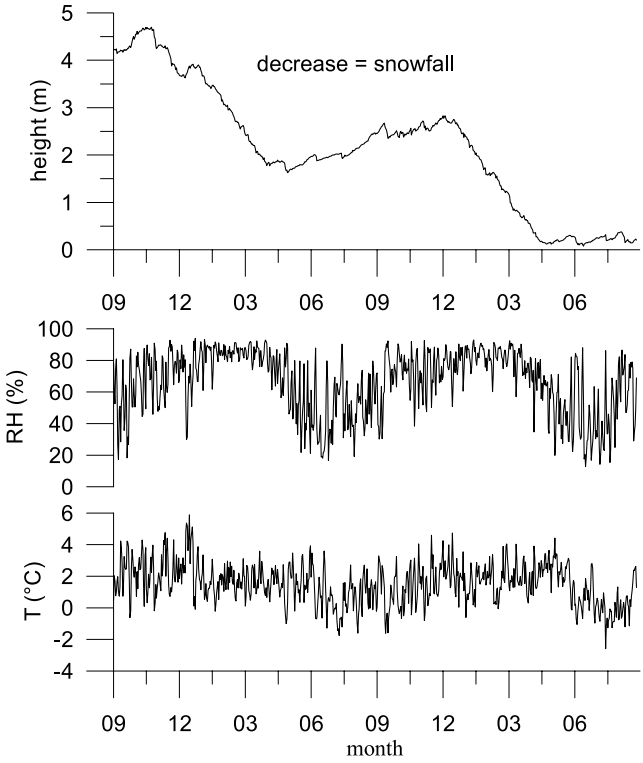

Figure 2. Daily measurements of the ultrasonic depth gauge at 2400 LT from September 1998 to August 2000 at 5150 m asl. A height increase is due to ablation or snowpacking; a height decrease is due to snowfalls. (bottom) Daily mean values of relative humidity and air temperature measured at 1.8 m above the surface outside the glacier at 4750 m asl.

[12] The potential solar irradiance is maximal from November to February, but its variations are small (Figure 4): The amplitude range of the daily values is 40% of the annual average, whereas at 45° latitude, this amplitude reaches 125% of the annual average. If short-term variations are disregarded, the solar irradiance at the glacier surface is fairly constant throughout the year; the high extraterrestrial irradiance of austral summer (wet season) is attenuated by frequent clouds (Figure 4). Because of atmospheric attenuation and shading of the surrounding mountains, about half of the annual extraterrestrial solar irradiance reaches the glacier surface (193 W m^{-2} over 391 W m^{-2}, annual averages at 5150 m asl in 1998–1999). This ratio is comparable for midlatitude glaciers [e.g., *Oerlemans and Knap*, 1998]. Tropical glaciers receive more solar radiation than midlatitude glaciers because of higher Sun elevation (low latitude) and larger atmospheric transmissivity (high altitude). The cloudless atmosphere reduces the potential solar radiation by about 80 W m^{-2} as a daily average (Figure 4). The minimal clear sky attenuation, when the Sun is close to the zenith, is around 10%.

4. Calculation of the Energy Balance

[13] The energy balance equation is an application of the law of conservation of energy on the vertical components, or the components perpendicular to the surface if the surface is tilted, of the energy fluxes at the glacier surface [e.g., *Kraus*, 1973; *Obled and Rosse*, 1977]:

$$R + H + \mathrm{LE} + P = \Delta Q_M + \Delta Q_S$$

$$\Delta Q_S = \int_0^{z^*} \frac{d(\rho c T)}{dt} dz \quad (1)$$

where R is the net radiation, H and LE are the turbulent fluxes of sensible and latent heat, respectively, and P is the heat advected by precipitation. The term ΔQ_S represents the change in heat content in a control volume and ΔQ_M is the energy used for melting (positive) or freezing (negative). The ice density and specific heat are ρ and c, respectively, and the ice temperature is T. The depth where the energy fluxes become nil is z^*. The fluxes are expressed in W m^{-2} and are counted as positive if they provide energy to the control volume. P remains very low on the Zongo Glacier and is neglected. We assume the fluxes R, H and LE are constant between the surface and the measurement height (surface sublayer depth of around 1 m).

[14] If the rates of change averaged over 0.5 hours are small, the steady state conditions can be assumed:

$$R + H + \mathrm{LE} = \Delta Q_M \quad (2)$$

4.1. Radiation

[15] The net radiation can be written as

$$R = S\downarrow - S\uparrow + L\downarrow - L\uparrow = S\downarrow (1 - \alpha) + L\downarrow \varepsilon - \varepsilon\sigma T_s^4 \quad (3)$$

where $S\downarrow$ is the short-wave irradiance or global radiation, $S\uparrow$ is the reflected short-wave radiation ($S = S\downarrow - S\uparrow$ is the net short-wave radiation), $L\downarrow$ and $L\uparrow$ are the long-wave irradiance and emittance, respectively ($L = L\downarrow - L\uparrow$ is the net long-wave radiation). The surface albedo is α, the long-wave emissivity of ice is ε, the Stefan-Boltzmann constant is $\sigma = 5.67\ 10^{-8}$ W m^{-2} K^{-4}, and the surface temperature is T_s. The ice emissivity ε is generally considered to be between 0.97 and 1.00 [*Kondratyev*, 1969; *Mellor*, 1977; *Dozier and Warren*, 1982; *Müller*, 1985]. The uncertainty on ε affects the "apparent" surface temperature: An emissivity decrease from 1 to 0.97 causes a 2°C increase in the apparent surface temperature in the range −10 to 0°C. We consider that ice is a full emitter ($\varepsilon = 1$), so that the reflection of long-wave radiation is neglected ($\alpha_{long\text{-}wave} = 1 - \varepsilon$). This assumption is acceptable considering the accuracy on long-wave radiation measurements (approximately ±10%).

[16] This study focused on the AWS2 at 5060 m asl. Two back-to-back pairs of CM3 pyranometers ($0.3 < \lambda < 2.8$ μm) and CG3 pyrgeometers ($5 < \lambda < 50$ μm) measured the four components of the net radiation (Table 1). A correction (K) is applied to the long-wave measurements to reduce the interference of solar radiation:

$$L\downarrow = L\downarrow_{measured} - KS\downarrow \quad (4)$$

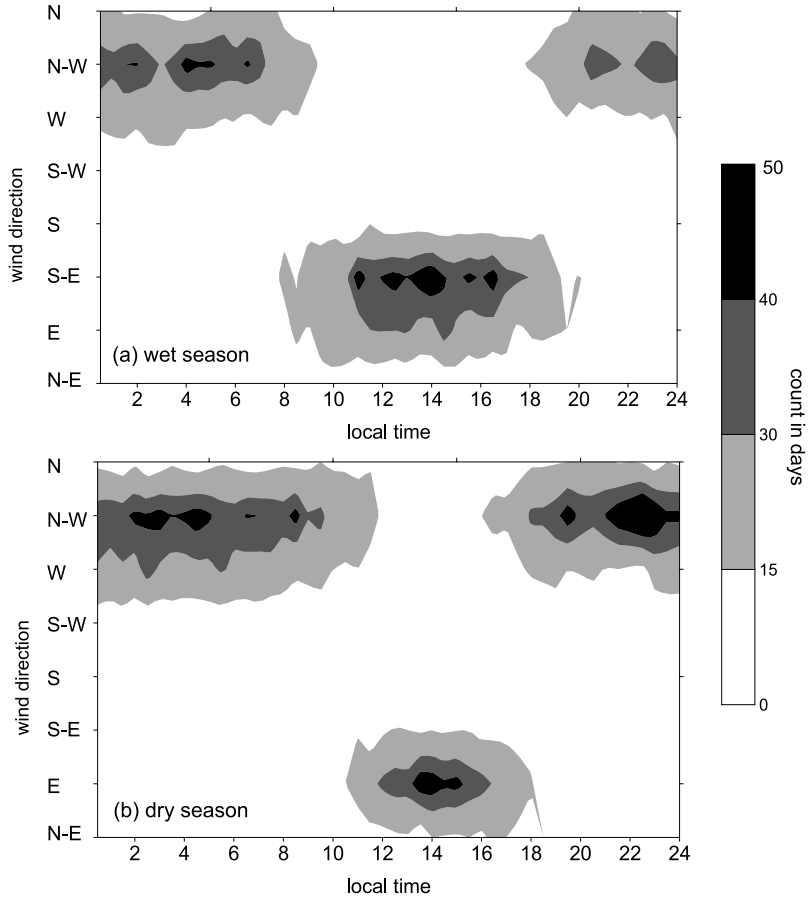

Figure 3. Wind direction (Y axis) versus hour of the day (X axis). Half-hourly values at 5150 m asl during the hydrological year 1999–2000 are shown. The shaded regions show the number of days. (a) Wet season (January to April). (b) Dry season (May to August).

[17] Analysis of $L\downarrow$ measurements under a shadowing ring (29 May 2002, clear sky) and of $L\uparrow$ measurements when the surface is melting at 0°C resulted in $K \approx 2\%$ on the Zongo Glacier. This result is close to the correction suggested by *Kipp and Zonen* [1995] and used by *Culf and Gash* [1993] and *Halldin and Lindroth* [1992], whereas *Obleitner and de Wolde* [1999] applied a smaller correction ($K = 1.2\%$). $L\uparrow$ measurements are limited to 316 W m^{-2}, corresponding to the ice emission at 0°C ($\varepsilon = 1$). The sensor height was too low (1 m) for the measurement of $L\uparrow$ to be disrupted by air emission [*Plüss and Ohmura*, 1997].

4.2. Turbulent Fluxes

[18] The turbulent heat fluxes were calculated with the bulk aerodynamic method, including stability correction. The stability of the surface layer is described by the bulk Richardson number Ri_b, which relates the relative effects of buoyancy to mechanical forces [e.g., *Moore*, 1983]:

$$Ri_b = \frac{g\frac{(T-T_s)}{(z-z_{0m})}}{T\left(\frac{u}{z-z_{0m}}\right)^2} = \frac{g(T-T_s)(z-z_{0m})}{Tu^2} \qquad (5)$$

where T and u are the air temperature (in K) and horizontal wind speed (in m s^{-1}), respectively, at the level of measurement z; g is the acceleration of gravity (g = 9.81 m s^{-2}), T_s is the surface temperature (in K, derived from $L\uparrow$), and z_{0m} is the surface roughness length for momentum (in m). Assuming that local gradients of mean horizontal wind speed u, mean temperature T, and mean

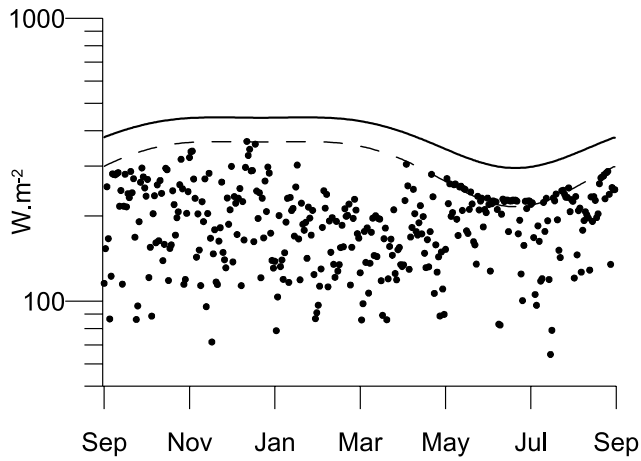

Figure 4. Daily mean values of global solar radiation measured at 5150 m asl (dots) and calculated extraterrestrial solar irradiance (solid line) from 1 September 1998 to 31 August 1999. The dashed line shows the extraterrestrial irradiance less 80 W m^{-2}.

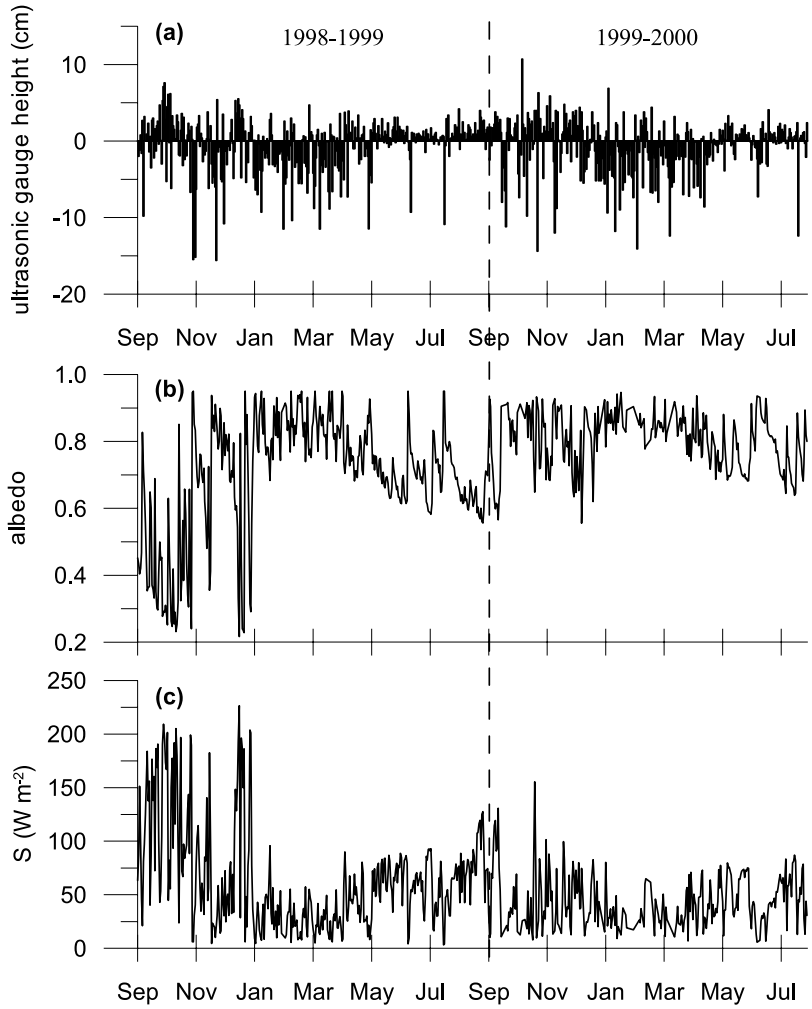

Figure 5. (a) Change in distance between the surface and the ultrasonic depth gauge. (b) Surface albedo. (c) Net short-wave radiation. Daily mean values at 5150 m asl (AWS1) from September 1998 to July 2000 are shown. Albedo is calculated from 0900 to 1500 LT to avoid shading from the surrounding mountains.

specific humidity q are equal to the finite differences between the measurement level and the surface, the turbulent fluxes are [*Brutsaert*, 1982]:

$$H = \rho \frac{C_p k^2 u (T - T_s)}{\left(\ln \frac{z}{z_{0m}}\right)\left(\ln \frac{z}{z_{0T}}\right)} (\Phi_m \Phi_h)^{-1} \tag{6}$$

$$\mathrm{LE} = \rho \frac{L_s k^2 u (q - q_s)}{\left(\ln \frac{z}{z_{0m}}\right)\left(\ln \frac{z}{z_{0q}}\right)} (\Phi_m \Phi_v)^{-1} \tag{7}$$

where q_s is the specific humidity at the surface (in g kg^{-1}, saturation is assumed), ρ is the air density, C_P is the specific heat capacity for air at constant pressure ($C_p = C_{pd}(1 + 0.84q)$ with C_{pd} = 1005 J kg^{-1} K^{-1}), L_s is the latent heat of sublimation of ice (L_s = 2.834 10^6 J kg^{-1}), and k is the von Karman constant (k = 0.4). The surface roughness lengths for temperature and humidity are z_{0T} and z_{0q}, respectively. The three roughness lengths are set equal to each other ($z_{0T} = z_{0q} = z_{0m}$) and are used as a calibration parameter to fit the calculated sublimation derived from LE to the measured sublimation with weighing lysimeters [*Wagnon et al.*, 1999]. During the period 1998–2000, no penitents (typical ablation forms observed on tropical glaciers [*Kotlyakov and Lebedeva*, 1974]) appeared and the roughness length varied from 1 to 5 mm.

[19] The nondimensional stability functions for momentum (Φ_m), heat (Φ_h), and moisture (Φ_v) are expressed in terms of Ri_b [*Webb*, 1970; *Brutsaert*, 1982]:

Ri_b positive (stable)

$$(\Phi_m \Phi_h)^{-1} = (\Phi_m \Phi_v)^{-1} = (1 - 5Ri_b)^2 \tag{8}$$

Ri_b negative (unstable)

$$(\Phi_m \Phi_h)^{-1} = (\Phi_m \Phi_v)^{-1} = (1 - 16Ri_b)^{0.75} \tag{9}$$

5. Results

5.1. Short-Wave Radiation

[20] Figure 5 compares the changes of surface height, measured by the ultrasonic depth gauge, with the surface

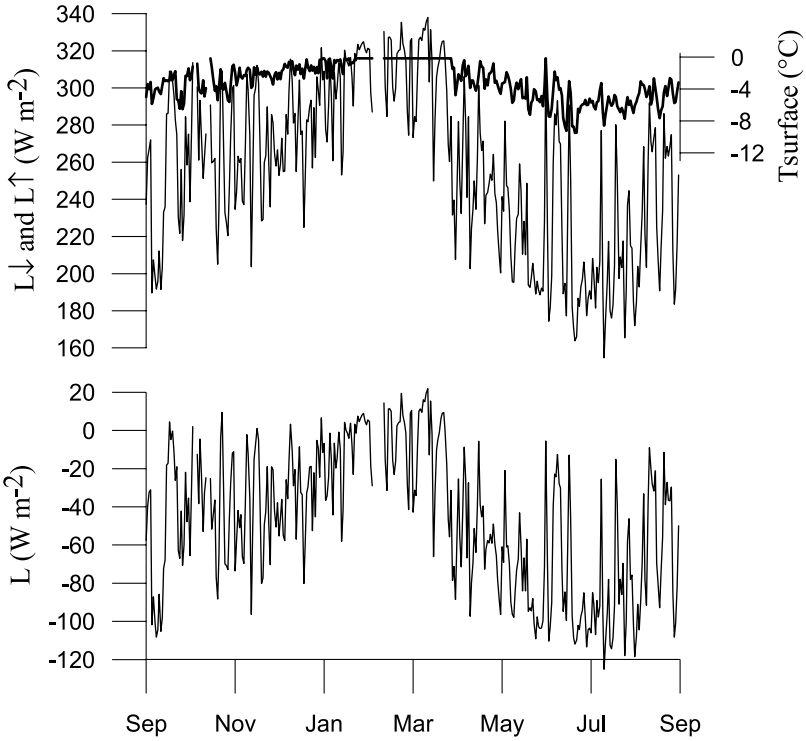

Figure 6. Daily mean values of the long-wave radiation fluxes at 5060 m asl during the hydrological year 1999–2000. (top) Irradiance ($L\downarrow$, thin line) and emittance ($L\uparrow$, thick line). Also shown is the surface temperature derived from $L\uparrow$ (right Y axis). (bottom) Net long-wave radiation (L).

albedo and the net short-wave radiation during the 1998–1999 and 1999–2000 hydrological years. The seasonal changes in extraterrestrial solar radiation are small at low latitudes and the net short-wave radiation at the glacier surface mainly depends on cloud cover and albedo, the latter related to snowfall and melting. From September to December, before the wet season actually got underway, snowfalls were scarce and rapidly melted in both years (Figure 5a). In 1998, ice appeared within a few days at 5150 m asl and the albedo dropped to values lower than 0.3 (Figure 5b). The solar radiation absorbed by the surface was high between September and December, particularly in 1998 because of a high snow line altitude (Figure 5c). Changes in net solar radiation in response to albedo fluctuations were often considerable from one day to another. Later, in the full wet season, from January to March, snowfalls were frequent enough to maintain a permanent snow cover at 5150 m asl and the albedo remained higher than 0.7. Because of high albedo and cloud cover, the net short-wave radiation remained rather low, around 50 W m^{-2}, despite the large potential solar irradiance (austral summer). Afterward, until the end of August, the smooth decrease of albedo to 0.6, corresponding to firn, was interrupted by rare snowfalls. In the dry season, the increase in solar radiation due to low cloud cover and decreasing albedo was partly compensated for by the decrease in potential solar radiation (austral winter). The net short-wave radiation was small, and progressively increased toward the September equinox.

5.2. Long-Wave Radiation

[21] Figure 6 shows the long-wave fluxes $L\downarrow$, $L\uparrow$ and L during the hydrological year 1999–2000. The net long-wave radiation was generally a large sink of energy for the surface, up to 120 W m^{-2}, except in the wet season when L was close to nil (maximum around +15 W m^{-2}). The surface emission varied little: between 280 and 316 W m^{-2} (mean value of 304 W m^{-2}), corresponding to mean surface temperatures ranging from −8°C in the dry season to 0°C in the wet season. The variations of L were controlled by the large fluctuations of $L\downarrow$ (coefficients of variation for $L\downarrow$ and $L\uparrow$ equal to 18 and 3%, respectively).

[22] The mean values of L in the wet (January to April 2000) and dry (May to August 2000) seasons were roughly −20 and −80 W m^{-2}, respectively. In the wet season, the long-wave irradiance was large because of the wet and warm atmosphere and the frequent clouds. In the dry season, the lowest values of $L\downarrow$ illustrate the dependence of the clear-sky emissivity on atmospheric temperature and humidity. As the clear-sky emission is low at high altitudes, the variations of $L\downarrow$ were considerable when clouds came in the dry season: Changes were up to 100 W m^{-2} from one day to another. The cloud emissions were greater for the low and warm cumulus or cumulonimbus of the wet season than for the high altostratus or cirrostratus of the dry season.

[23] Figure 7 shows the hourly surface temperature and net long-wave radiation during the hydrological year 1999–2000. At 5060 m asl, the surface reached the melting conditions almost every day of the year (Figure 7a). The glacier surface remained close to the melting conditions,

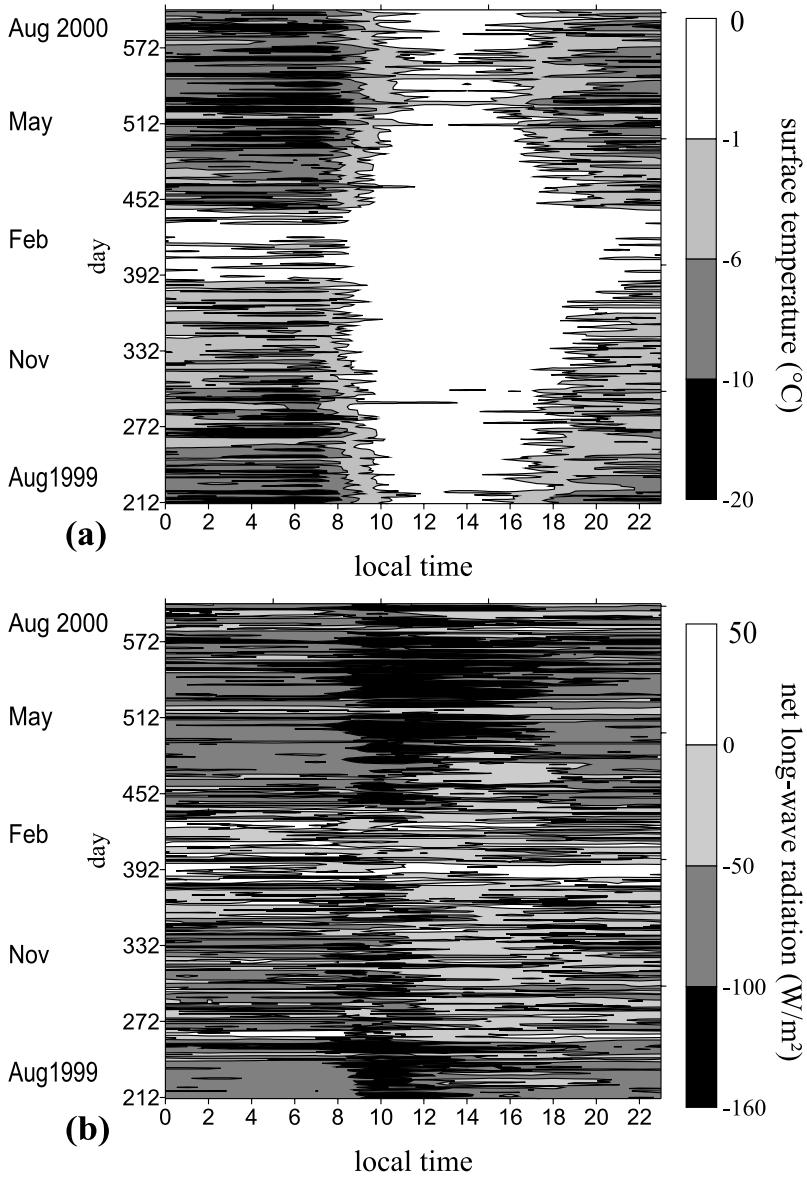

Figure 7. Hourly values of (a) surface temperature and (b) net long-wave radiation measured at 5060 m asl from August 1999 to August 2000. Local time is shown on the *X* axis, and day of the year is shown on the *Y* axis.

day and night, in the core of the wet season from January to March. In the dry season, the daily amplitude of the surface temperature was maximal (10–15°C) and the surface melted for only a few hours in the afternoon.

[24] At night, any increase of $L\downarrow$ due to clouds caused an increase of the surface temperature, and therefore of the emittance. The nocturnal radiation deficit ($L < 0$), larger in the dry season (Figure 7b), was balanced by the energy income from the turbulent fluxes and/or from the cooling of ice beneath the surface (see sections 5.3 and 5.4). During diurnal melting, clouds enhanced $L\downarrow$, whereas the emittance remained constant at 316 W m^{-2}; the surface temperature could only decrease from the melting point. At night, the surface temperature fluctuated greatly and the net long-wave radiation varied little, whereas once the surface temperature reached its upper limit at 0°C during the daytime, the net long-wave radiation varied with the cloud cover. As a result, L was maximal during the cloudy afternoons of the wet season (Figure 7b). L was minimal in the dry season, when the incoming flux $L\downarrow$ was small, and in the afternoon when the emission temperature was maximal (Figure 7b).

5.3. Turbulent Fluxes

5.3.1. Vertical Thermal Profile

[25] *Wagnon et al.* [1999] observed an air temperature maximum within the first meter above the surface of the Zongo Glacier during a clear-sky period in 1997. This thermal anomaly can cause a significant change in sensible heat flux with height. Whereas Wagnon's observations were based on a few days, Figure 8 shows the mean vertical thermal profiles over 2 months of the dry season 2000.

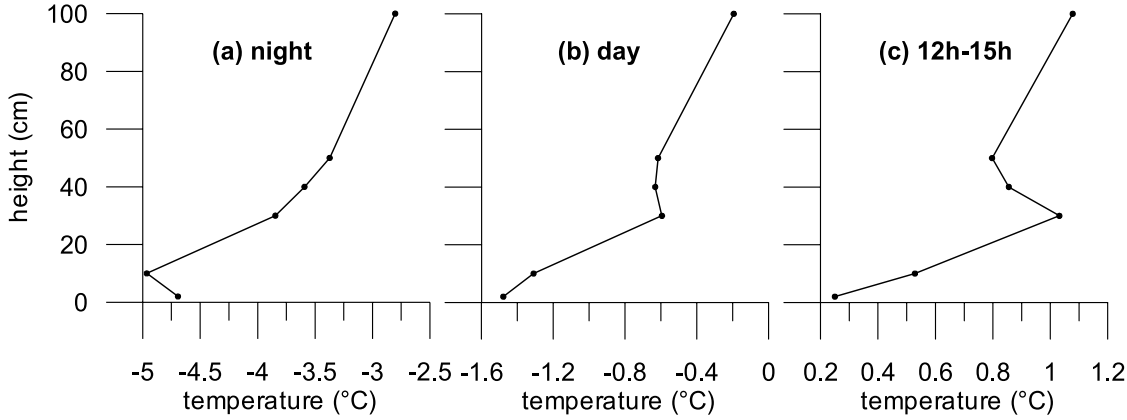

Figure 8. Vertical profiles of aspirated air temperature at 5150 m asl from 1 June to 31 July 2000. (a) Nocturnal mean profile between 1800 and 0600 LT (4320 data). (b) Diurnal mean profile between 0600 and 1800 LT (4320 data). (c) Mean profile between 1200 and 1500 LT (1080 data).

During the daytime, the stable profile was disrupted by high temperatures at 30–40 cm above the surface, which reached their maximal values in the afternoon (Figures 8b and 8c). The "warm layer" occurred quite often: A temperature maximum appeared between 10 and 40 cm above the surface for 20% of the daytime data from June and July 2000. The thermocouples were shielded from the solar radiation and artificially ventilated (section 2). The mean nocturnal profile indicates a correct intercalibration of the sensors (Figure 8a). The anomalous high nocturnal temperatures recorded at the lowest level (2 cm above the surface) were probably due to snow accumulation in the sensor. The potential effects of the warm layer on the turbulent flux measurements are discussed in section 6.1.

5.3.2. Diurnal Cycles

[26] Figure 9 shows the mean diurnal cycles of wind speed, bulk Richardson number, temperature, specific humidity, and turbulent fluxes during the wet and dry seasons of the hydrological year 1999–2000. The wind speed was greater in the dry season (average of 3.3 m s^{-1}) than in the wet season (average of 2.2 m s^{-1}), essentially because of a stronger glacier wind (Figures 3 and 9a). The valley wind caused a wind speed maximum in the afternoon, more pronounced in the wet season (Figure 9a). The air flow was thermally stable most of the time and close to neutral conditions in the afternoon (Figure 9b). The air was slightly more stable in the dry season than in the wet season as a result of the counteracting effects of lower surface temperatures and stronger winds on stability (Figures 7a, 9a, and 9b). In the wet season, both glacier and air temperatures fluctuated around 0°C, producing small vertical thermal gradients (Figure 9c). In the dry season, the surface was much colder than the air, essentially because of the deficit in long-wave radiation (Figure 7) associated with katabatic drainage (Figures 3 and 9a). The thermal gradient was small only in the afternoon, when the air and the glacier were both close to 0°C (Figures 9c). The vertical gradient of specific humidity was generally negative (sublimation) (Figure 9d). In the wet season, humid air close to 0°C flowed over the melting surface, producing small humidity gradients. The air was colder and drier in the dry season. During the nights of the dry season, low surface temperatures caused low saturating humidity, leading to small humidity gradients between the surface and the air (Figure 9d). During the afternoons of the dry season, the saturating humidity at the melting surface was high, whereas the air was dry, causing strong negative gradients of humidity (Figure 9d).

[27] Because of light wind and small thermal and humidity gradients, the sensible (positive) and latent (sublimation) heat fluxes were small in the wet season (H and $-$LE $\sim$ 10 W m^{-2}, Figure 9e). They canceled each other out, so that the sum of the turbulent fluxes was very small (Figure 9f). The magnitude of each turbulent flux was greater in the dry season than in the wet season because of stronger wind and higher thermal and humidity gradients, and despite slightly greater air stability (Figure 9e). During the night and the morning, both turbulent fluxes canceled each other out, so that the sum was as small as in the wet season (Figure 9f). In the afternoon, small thermal gradients reduced the sensible heat flux (Figure 9c), whereas large humidity gradients (Figure 9d) caused a large sublimation (around -100 W m^{-2}) (Figure 9e). As a result, the turbulent fluxes were a large sink of energy during the afternoons of the dry season (around -80 W m^{-2}) (Figure 9f).

5.3.3. Daily Values

[28] Figure 10 shows the relationships between the turbulent fluxes and air temperature, vapor pressure and wind speed on the daily timescale. The largest daily sensible and latent heat fluxes were around +100 W m^{-2} (8.6 M J d^{-1}) and -200 W m^{-2} (-17.2 M J d^{-1}), respectively. We found no relationship between the turbulent fluxes and air temperature (Figures 10a and 10d) because any warming of the air enhances stability. H and LE increased in magnitude when the wind speed (humidity) increased (decreased) (Figures 10b and 10c). The sum H + LE was generally negative and tended to decrease in intensity when the vapor pressure increased (Figure 10e) or when the wind speed decreased (Figure 10f).

[29] The latent heat flux accounted for most of the variations of the sum H + LE because LE was more variable and generally larger than H (r^2(LE, H + LE) = 0.64, r is correlation coefficient). H and LE are strongly anticorrelated (r^2(LE, H) = 0.79) because the wind accounts for 70–80% of the fluctuations of each flux. The apparent increase

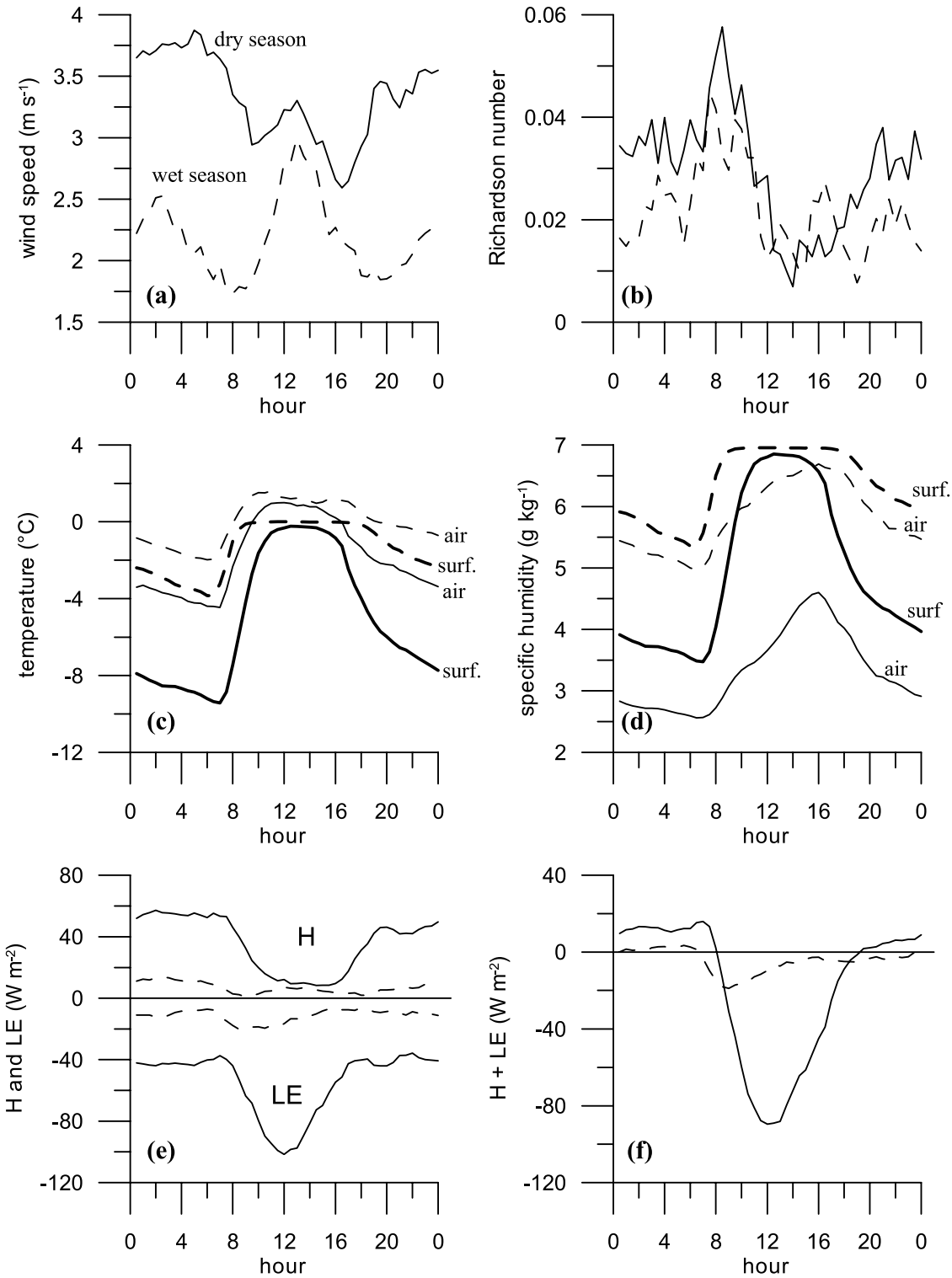

Figure 9. Mean daily cycle of (a) wind speed, (b) bulk Richardson number, (c) air and surface temperature, (d) air and surface specific humidity, (e) turbulent sensible (H) and latent (LE) heat fluxes, and (f) the sum H + LE on the glacier at 5060 m asl. The dashed (solid) lines show the mean cycle during the wet season of November 1999 to February 2000 (during the dry season of May to August 2000). In Figure 9c (Figure 9d) the thick and thin lines show the surface and air temperature (humidity), respectively.

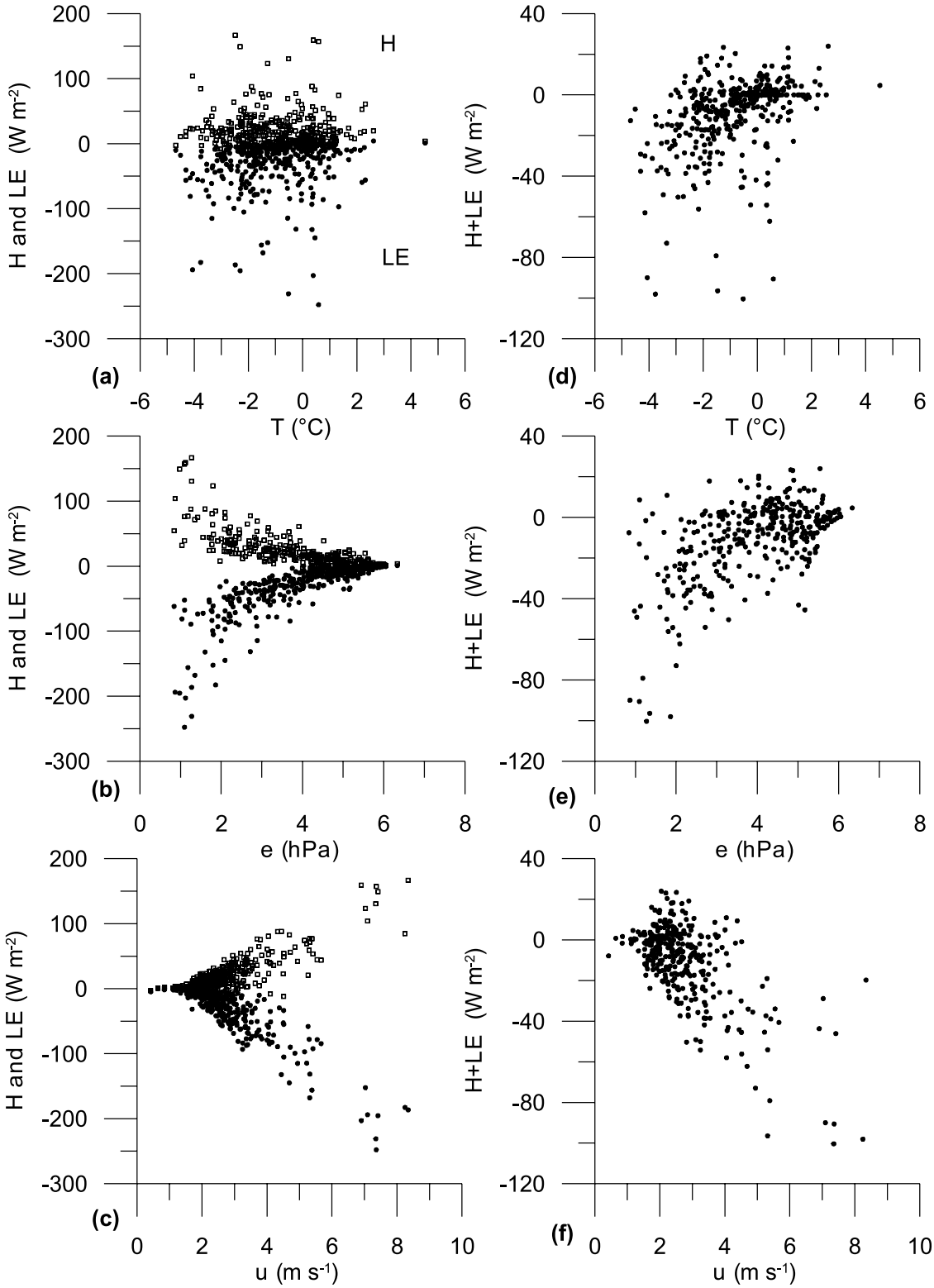

Figure 10. Turbulent sensible (H) and latent (LE) heat fluxes as a function of air temperature T, vapor pressure e, and wind speed u. Daily mean values at 5060 m asl over the hydrological year 1999–2000 are shown. H (open squares) and LE (solid dots) versus (a) T, (b) e, and (c) u. H + LE versus (d) T, (e) e, and (f) u.

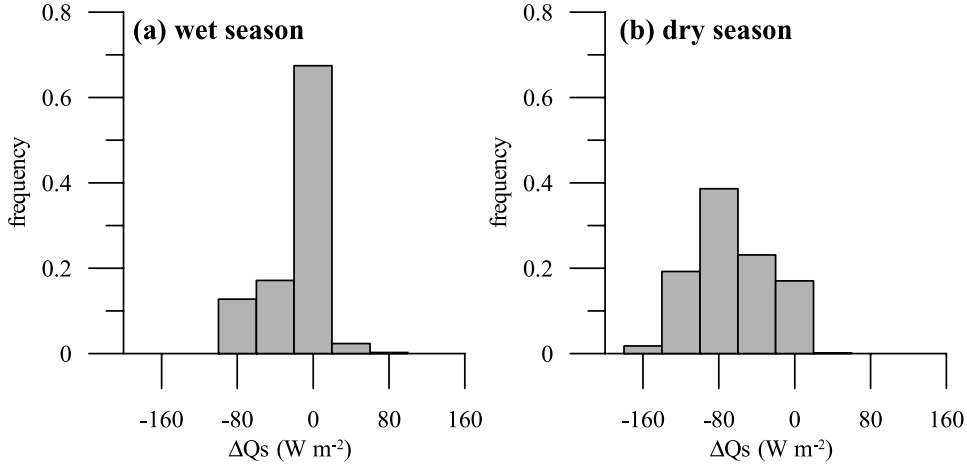

Figure 11. Subsurface heat content (ΔQ_S) calculated from equation (1). Half-hourly mean values between 2400 and 0500 LT ($\Delta Q_M = 0$) are shown. (a) From December to January 2000 (600 values). (b) From June to July 2000 (610 values).

in sensible heat flux with air dryness (Figure 10b) is due to the negative correlation between humidity and wind speed, since the wind is stronger in the dry season (Figure 9a).

5.4. Subsurface Heat Flux

[30] The ablation area of the Zongo Glacier is isothermal at 0°C except for a superficial layer of a few tenths centimeter thick, which undergoes seasonal thermal fluctuations. In absence of phase change ($\Delta Q_M = 0$), the energy fluxes only cause changes in heat content of the ice (ΔQ_S). Figure 11 shows ΔQ_S derived from the energy balance in the middle of the night. As uncertainties are large on ΔQ_S as residual of equation (1), only the main differences between the wet and dry seasons are discussed.

[31] During the cloudy nights of the wet season, the radiation and turbulent budgets were close to nil (Figures 7b and 9f) and the amount of available energy

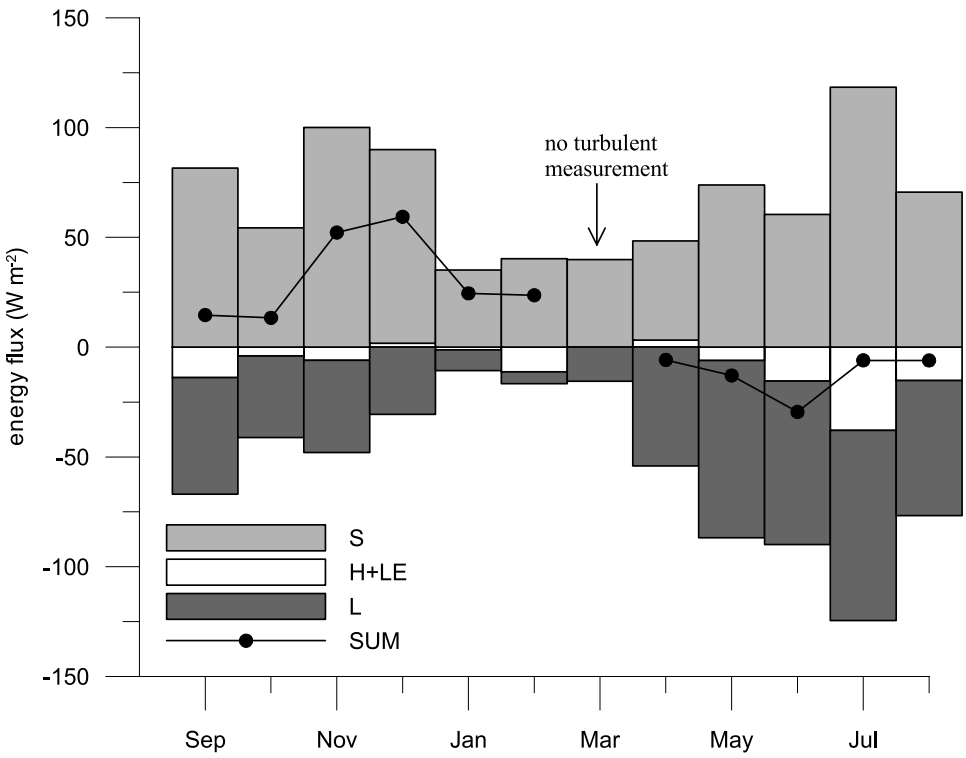

Figure 12. Monthly averages of the energetic fluxes at 5060 m asl over the hydrological year 1999–2000. S is the net short-wave radiation, H + LE is the sum of the turbulent sensible and latent heat fluxes, and L is the net long-wave radiation. SUM is the sum of the fluxes. No turbulent data are available for March because of sensor breakdown.

Table 2. Monthly Averages of Energy Fluxes at 5060 m asl Over the Hydrological Year 1999–2000[a]

	H	LE	S	L	Sum
Sept.	21	−35	82	−53	15
Oct.	16	−20	54	−37	13
Nov.	17	−23	100	−42	52
Dec.	10	−8	88	−31	59
Jan.	2	−3	35	−9	25
Feb.	0	−10	40	−5	25
March	no data	no data	40	−16	
April	12	−9	45	−54	−6
May	33	−39	74	−81	−13
June	50	−66	60	−74	−30
July	29	−67	118	−87	−6
Aug.	31	−46	71	−62	−6

[a]Energy fluxes are in W m^{-2}. No turbulent data are available for March because of sensor breakdown.

was small: ΔQ_S ranged from −40 to +40 W m^{-2} for 70% of the data (Figure 11a). During the clear-sky nights of the dry season, the long-wave radiation budget was negative (emittance larger than irradiance) (Figure 7b) and the turbulent fluxes were small (Figure 9f): The sum of the atmospheric energy fluxes was generally negative (average of −66 W m^{-2}) (Figure 11b) and the surface was cold. The large temperature gradients in the ice caused a conductive heat flux from the subsurface layers; the cooling of ice tended to compensate the deficit in energy at the surface ($\Delta Q_S < 0$) (Figure 11b).

[32] A conductive heat flux of 60 W m^{-2} can result from a thermal gradient of 28 K m^{-1} in the ice (thermal conductivity $K_{ice} \approx 2.10$ W m^{-1} K^{-1}) or of 75 K m^{-1} in old snow ($K_{snow} \approx 0.80$ W m^{-1} K^{-1}). *Wagnon et al.* [2003] measured similar thermal gradients, around 100 K m^{-1}, in the first centimeters of snow at the summit of the Illimani (6340 m asl, Bolivia).

5.5. Annual Cycle of the Energy Fluxes

[33] Figure 12 and Table 2 show the annual cycle of the energy fluxes at 5060 m asl. As H is anticorrelated to LE through the wind speed, Figure 12 compares the sum of the turbulent fluxes with the net short-wave and net long-wave radiation fluxes. Most of the year, H and LE tended to cancel each other out, so that the sum of the turbulent fluxes remained small, except in the dry season when H + LE was a significant loss of energy due to strong wind and dry air: H + LE ≈ −40 W m^{-2} in July (−100 MJ m^{-2}). The net short-wave radiation varied with the cloud cover and the albedo, without following any marked annual cycle. In contrast, the net long-wave radiation varied from very negative values in the dry season, due to a cold and dry atmosphere, to values close to nil in the wet season due to cloud emissions (Table 2).

[34] The melting energy mainly depends on the balance between the solar energy input and the long-wave radiation output. The sum of the atmospheric energy fluxes at 5060 m asl was positive in the wet season (September to March), the maximum was between November and December: H + LE + S + L ≈ +50–60W m^{-2}, and was slightly negative in the dry season (April to August). However, the errors on each flux accumulate in the sum; as a result, the amount of available energy contains substantial uncertainties and its sign was uncertain in April, July, and August 2000 (Table 2).

6. Discussion

6.1. Uncertainties on the Turbulent Fluxes

[35] The radiation measurements are robust compared to the turbulent fluxes derived from the profile method. Since H and LE generally are of opposite signs, the total turbulent fluxes result from the difference between two terms of similar magnitude and associated with large errors, so that even the sign of H + LE can be uncertain.

[36] There is no consensus on the validity of the log linear corrections (equation (8)) in very stable stratification [e.g., *Webb*, 1970; *Andreas*, 2002], but stability is generally moderate on the Zongo Glacier (Figure 9b) ($Ri_b > 0.1$ for only 8% of the half-hourly values). The roughness lengths are a greater source of uncertainty. We chose to use a single roughness length based on LE and lysimeter measurements (z_{oq}). The lengths z_{oT} and z_{oq} are expected to be smaller than z_o for rough surfaces [e.g., *Brutsaert*, 1982], but this did not affect the calculations of H and LE on the Zongo Glacier because z_o was used as a calibration factor for LE, similar to the ''effective'' roughness of *Braithwaite* [1995]. The resulting roughness length z_o depends on the local experiment. This method allows for calibrating the latent heat flux, but the ratio z_{oT}/z_{oq} is not constrained; the Bowen ratio H/LE is not well known. Since it is difficult to measure humidity gradients above glacier surfaces, few studies have investigated the relationship between z_{oT} and z_{oq}. Some measurements suggested large differences between z_{oT} and z_{oq} [e.g., *Smeets et al.*, 1998; *Meesters et al.*, 1997;], but most authors considered equality [e.g., *Hay and Fitzharris*, 1988; *Munro*, 1989; *Bintanja and Van den Broeke*, 1995; *Zuo and Oerlemans*, 1996; *Hock and Holmgren*, 2005]. *Andreas* [1987] argued that heat and moisture are transferred by similar processes above snow and ice, so that z_{oq} and z_{oT} must be similar.

[37] The uncertainties on the lysimeter measurements are difficult to assess. The errors mainly stem from the disturbance of the snow surface, the disruption of the flux of water vapor in the snow at the bottom of the lysimeter (roughly 10 cm deep), and snow scouring by wind. On the Zongo Glacier, the standard error on the mean of the measurements of seven lysimeters was only around 0.15 mm w.e. per day in August 2004.

[38] A ''warm layer'' regularly appears within the first meter above the glacier surface by cloudless sky and light wind (see section 5.3.1). The divergence of sensible heat at low height may undermine the assumption of a constant vertical flux layer, making the bulk method inappropriate for measuring turbulent fluxes at the glacier surface. A few authors observed this kind of thermal anomaly above melting snow [*de la Casinière*, 1974; *Martin*, 1975; *Halberstam and Schieldge*, 1981; *Male and Granger*, 1981; *Meesters et al.*, 1997]. The processes involved were not clearly identified: probably solar or long-wave radiation absorption by water vapor and/or aerosol particles. As the warm layer appears when the wind is light and the turbulent exchanges are small, the error probably does not have a strong impact on the overall energy balance calculations. Likewise, the error on air tempera-

ture due to the absence of artificial ventilation at AWS2 must have a limited impact on the turbulent fluxes that are small when the wind speed is not sufficient to ventilate the sensors. The error on T_s derived from the surface emittance in long-wave radiation is certainly greater.

[39] Glacier wind, frequent on the Zongo Glacier (Figure 3), is characterized by a wind speed maximum at low height, generally at less than 10 m above of valley glaciers, which causes a divergence of horizontal momentum [e.g., *Kuhn*, 1978; *Martin*, 1975; *Greuell et al.*, 1997; *Oerlemans and Grisogono*, 2002]. According to *Denby and Greuell* [2000], the constant vertical flux layer is reduced to a few tens of centimeters deep when the wind maximum is at 5 m above the surface. In this case, the Monin-Obukhov similarity theory is not applicable because the turbulent transport term of the turbulent kinetic energy balance is not negligible at proximity of the height of the wind maximum. The glacier wind properties have been studied in detail on midlatitude and on high-latitude glaciers [e.g., *Munro and Davies*, 1978; *Van den Broeke*, 1997; *Smeets et al.*, 1998; *Van der Avoird and Duynkerke*, 1999]. Wind profile observations are very rare on small tropical glaciers. At 5150 m asl on the Zongo Glacier, the wind speed at 180 cm above the surface was lower than at 30 cm for 15% of the nocturnal measurements in 1999–2000 (1800–0600 LT), implying a wind speed maximum at less than 180 cm above the surface. Moreover, the usual pattern of stronger wind at 180 than at 30 cm above the surface does not mean there was not a wind maximum between both sensor levels.

[40] As the turbulent exchanges are enhanced in the glacier wind, the inappropriate level of measurement relative to the glacier wind speed maximum and the uncertainty on the roughness lengths z_{oT}/z_{oq} are probably the main sources of error on the turbulent fluxes, which are not known with an accuracy better than ±20%.

6.2. Surface Energy Fluxes at Very High Altitude

[41] The high-altitude atmospheric specificities of midlatitude mountains, where most meteoglaciological studies have been conducted, are exacerbated in the very high tropical mountains. Taking into account the thicker atmosphere at low latitudes [e.g., *Prohaska*, 1970], approximately half of the atmospheric mass is below the Zongo Glacier.

[42] The atmospheric attenuation and diffusion of solar radiation is low at high altitudes because of small concentrations of water vapor and aerosol. On the Zongo Glacier, the clear-sky solar irradiance is at 90% in direct radiation and can exceed 85% of the extraterrestrial solar irradiance. The large direct component of $S\downarrow$ favors the growth of penitents [*Kotlyakov and Lebedeva*, 1974]. The ultraviolet band is absorbed by stratospheric ozone, whereas the near infrared is mainly absorbed by water vapor at low altitudes. The spectral shift of solar radiation with elevation can affect the snow albedo, which is strongly spectrally dependent.

[43] Because of the thin atmosphere, the long-wave irradiance is small on tropical glaciers: $L\downarrow$ varies from 180 to 340 W m^{-2}, whereas $L\downarrow$ generally ranges from 240 to 380 W m^{-2} on midlatitude glaciers [e.g., *Greuell et al.*, 1997; *Olyphant*, 1986]. The clear-sky emissivity is very low: The minimum is around 0.5 on the Zongo Glacier, which is lower than the emissivity of around 0.6–0.7 of the cold atmosphere of Antarctica, as reported by *Van den Broeke et al.* [2004]. The transmission of cloud radiation through the air is mainly in the 8–14 μm atmospheric window, where water molecules absorb and emit, so that cloud contributions to the surface long-wave irradiance increases in cold and dry air [*Kimball et al.*, 1982]. In the dry atmosphere of the high-altitude tropical glaciers, clouds can increase the long-wave radiation by more than 50% (Figure 6), whereas this enhancement remains less than 30–40% at midlatitudes [*Kimball et al.*, 1982]. Thus changes in atmospheric temperature (cloud cover) have smaller (greater) effects on the net long-wave radiation of tropical glaciers than on midlatitude glaciers.

[44] The slight decrease of the melting temperature of ice with elevation has a negligible effect on the long-wave emittance of glaciers. Finally, at high elevations, the light air carries less heat, which partly explains the small sensible heat fluxes observed on the Zongo Glacier (see section 5.3).

[45] The measurement methods can be altered by elevation. For example, the psychrometers are based on [*Queney*, 1974]

$$e = e_w(T_m) - Ap(T - T_m), \tag{10}$$

where $A \sim 66°C^{-1}$ depends on the wind speed, e is the vapor pressure, $e_w(T_m)$ is the saturation vapor pressure at temperature T_m, T, and T_m are the dry and wet air temperature, respectively, and p is the atmospheric pressure. As p is only around 500 hPa at the elevation of tropical glaciers, the contribution of the term $(T - T_m)$ to the humidity measurement is only half of its contribution at sea level (equation (10)). The psychrometric method, based on the difference between the dry and the wet temperatures, is not well adapted to the high tropical mountains: Elevation lessens the sensitivity of the sensor. Thus on the Zongo Glacier, capacitive hygrometers replaced the psychrometers at the AWS1 in 1999. The psychrometer measurements used by *Wagnon et al.* [1999] were biased toward overly high air humidity. As LE was calibrated on lysimeter measurements, the height z_0 was overestimated to compensate for humidity gradients that were too small.

6.3. Seasonal and Interannual Variability in Melting

[46] *Ohmura* [1990], *Kaser et al.* [1996], and *Wagnon et al.* [1999] emphasized the importance of ice sublimation as a favorable factor for the existence of high-altitude glaciers by limiting the energy available for melting. However, this study shows that long-wave radiation plays a more important role in the seasonal changes of the ablation of tropical glaciers (Figure 12). Penitents are often considered as indicators of the importance of the sublimation in the annual cycle of melting. However, the height and duration of penitents are highly variable on tropical glaciers, whereas melting is very low every year in the dry season, independently of whether penitents that drastically change the turbulent flux magnitude appear.

[47] The energy loss by turbulent fluxes is significant only in the dry season, when the glacier wind prevails most of the day. The energy deficit in long-wave radiation is

larger and reduces melting every time the atmosphere is cloudless and solar radiation is high: in the dry season, but also when the energy inputs are large at the beginning of the hydrological year (Figure 12). In the core of the wet season, from January to March or April, cloud emissions offset most of the glacier emission, so that melting is maintained despite the high albedo of fresh snow. Over the year, a strong correlation exists between the daily averages of $L\downarrow$ and $L\uparrow$ ($L\uparrow = 252 + 0.19\ L\downarrow$, $r^2 = 0.75$). This confirms that clouds (related to $L\downarrow$) have a strong influence on the energy balance, since the surface temperature ($L\uparrow$), when negative, integrates all the energy fluxes. The sky long-wave radiation directly depends on cloud cover and humidity, which are the main seasonal variables of low-latitude climates. Furthermore, the cloud cover's control on L is enhanced in the thin atmosphere of high-altitude mountains (see section 6.2).

[48] Related to the cloud cover, snowfalls reduce the melting energy through a rapid increase of the surface albedo. The period of substantial melting from September to December, due to high solar radiation and low surface albedo, is interrupted by the frequent snowfalls that characterize the core of the wet season. The arrival of frequent clouds and snowfalls around January is a key period for snow accumulation, but also for the ablation of the tropical glaciers.

[49] Neither the temperature nor the humidity is the limiting factor for the turbulent fluxes that are mainly controlled by wind. The relations between the wind at the glacier surface and the regional climate are complex. To assess the response of the surface energy balance to climatic changes, one approach is to investigate the potential disruption of the diurnal cycle of the wind regime; on the Zongo Glacier, the valley and glacier winds are related to distinct patterns of H and LE.

[50] The ablation area remains close to the melting conditions during the wet season, which allows for a reliable closure of the energy budget at the glacier surface. In the dry season, the daytime energy inputs progressively offset the large subsurface cold content accumulated during the night (Figure 7), so that melting, if any, is delayed. The monthly sum of the energy fluxes can be negative from June to August (Figure 12), which does not prevent some melting at the surface because of the low thermal conductivity of ice. The delay in melting is also expected at the onset of the wet season because of the cold content accumulated throughout the dry season, as during spring in midlatitude glaciers.

[51] It is not surprising that the mean atmospheric temperature and humidity are not clearly linked to the mass balance of tropical glaciers (see Introduction), which are surrounded by a very dry and thin atmosphere. The El Niño–Southern Oscillation (ENSO) warm phase prevailed during the last two decades of the 20th century, leading to frequent El Niño events, but several observations pointed out a likely shift to the cold phase regime in the late 1990s [*Trenberth and Hoar*, 1996; *Fedorov and Philander*, 2000]. During an El Niño event the wet season is delayed in Bolivia, the period of strong melting by solar radiation around the summer solstice lasts longer (Figure 5), and the mass balance of glaciers is highly negative. El Niño events also cause high ablation on equatorial glaciers due to high-altitude liquid precipitations [*Favier et al.*, 2004]. How the El Niño frequency may change in a warmer climate is an open question [e.g., *Huber and Caballero*, 2003].

7. Summary and Conclusion

[52] This study analyzed the energy fluxes at the surface of the tropical Bolivian Zongo Glacier in order to identify the atmospheric variables that control the seasonal variations of melting. Measurements taken from 1998 to 2000 at two meteorological stations at 5150 and 5060 m asl were examined.

[53] In the outer tropics, the progressive buildup of the wet season, from September to January, is a period of high energy inputs: The solar irradiance is close to its austral summer peak, clouds and snowfalls are still sporadic, and the glacier albedo is low. The core of the wet season generally lasts from January to April. Clouds reduce solar irradiance and snowfalls cause a high albedo, whereas the glacier deficit in long-wave radiation is low because of the emission of low and warm convective clouds, so that melting energy is moderate. The amount of available energy is very small in the dry season, from May to August, essentially because of the high deficit in long-wave radiation in a dry atmosphere, but also because of the energy loss in sublimation. Over the year, the radiation fluxes account for most of the energy balance of the tropical glaciers, and the solar energy is, by far, the main source of energy.

[54] In the dry season, the ablation area is close to melting conditions for only a few hours in the afternoon, and the nocturnal surface temperatures are low (-10 to -15°C), whereas the surface remains around 0°C throughout the wet season. High-altitude tropical glaciers are characterized by the marked seasonality of the net long-wave radiation because cloud emissions drastically enhance the low long-wave emittance of the thin atmosphere. The deficit in long-wave radiation is maximal during clear-sky days, counteracting the maximal energy inputs. Directly linked to cloud cover and humidity, the main seasonal control factors of low-latitude climates, long-wave radiation is a key variable of the energy balance of tropical glaciers.

[55] On tropical glaciers, ablation is closely linked to accumulation: The high albedo of fresh snow in the wet season interrupted the period of large solar energy around the summer solstice of December. Any delay in the wet season, such as during an El Niño event, causes a very negative mass balance due to low accumulation and high ablation.

[56] The turbulent flux of sensible heat is generally a gain in energy for the glacier surface, whereas the latent heat flux is a sink (sublimation). The sensible heat flux is less important on tropical glaciers than on midlatitude glaciers because of smaller temperature gradients and air density. Both turbulent fluxes tend to cancel each other out all year round, except during the daytime in the dry season when sublimation prevails because of strong wind and dry air. The turbulent fluxes are still poorly known on tropical glaciers: Eddy correlation measurements associated with wind, temperature and humidity profiles would give better insights on the roughness lengths, the stability functions, and glacier wind properties.

[57] Near the snow line, the albedo varies greatly over short distances, so that the interpretation of punctual energy

flux measurements can lead to an erroneous generalization of the melting characteristics to the entire ablation area. A distributed energy balance model is required to relate the atmospheric forcing to the mass balance of tropical glaciers.

[58] **Acknowledgments.** The glaciological program is supported by l'Institut de Recherche pour le Développement (IRD). The authors are grateful for the assistance received from IHH (Instituto de Hidraulica e Hídrologia), UMSA (Universidad Mayor de San Andrés) in La Paz, and from the Laboratoire de Glaciologie et Géophysique de l'Environnement in Grenoble (LGGE, CNRS). We are grateful to Jean-Philippe Chazarin, Robert Gallaire, and Alvaro Soruco for the fieldwork and the meteorological stations maintenance. J.E. Sicart was supported by the NERC Standard Grant NER/A/S/2001/01089. This work is sponsored by the French ORE network Glacioclim and the ACI C3 "Changement Climatique et Cryosphère" (C. Genthon, LGGE). The authors are also grateful to two anonymous reviewers for making useful comments on the manuscript.

References

Andreas, E. L. (1987), A theory for the scalar roughness and the scalar transfer coefficients over snow and sea ice, *Boundary Layer Meteorol.*, *38*, 159–184.

Andreas, E. L. (2002), Parameterizing scalar transfer over snow and ice: A review, *J. Hydrometeorol.*, *3*, 417–432.

Bintanja, R., and M. Van den Broeke (1995), The surface energy balance of Antarctic snow and blue ice, *J. Appl. Meteorol.*, *34*, 902–926.

Braithwaite, R. J. (1995), Aerodynamic stability and turbulent sensible-heat flux over a melting ice surface, the Greenland ice sheet, *J. Glaciol.*, *41*, 562–571.

Brutsaert, W. (1982), *Evaporation into the Atmosphere: Theory, History and Applications*, 1st ed., 299 pp., Springer, New York.

Chen, J., B. E. Carlson, and A. D. Del Genio (2002), Evidence for strengthening of the tropical general circulation in the 1990s, *Science*, *295*, 838–841.

Culf, A. D., and J. H. C. Gash (1993), Longwave radiation from clear skies in Niger: A comparison of observations with simple formulas, *J. Appl. Meteorol.*, *32*, 539–547.

de la Casinière, A. C. (1974), Heat exchange over a melting snow surface, *J. Glaciol.*, *13*, 55–72.

Denby, B., and W. Greuell (2000), The use of bulk and profile methods for determining surface heat fluxes in the presence of glacier winds, *J. Glaciol.*, *46*, 445–452.

Dozier, J., and S. G. Warren (1982), Effect of viewing angle on the infrared brightness temperature of snow, *Water Resour. Res.*, *18*, 1424–1434.

Favier, V., P. Wagnon, J. P. Chazarin, L. Maisincho, and A. Coudrain (2004), One-year measurements of surface heat budget on the ablation zone of Antizana glacier 15, Ecuadorian Andes, *J. Geophys. Res.*, *109*, D18105, doi:10.1029/2003JD004359.

Fedorov, A. V., and S. G. Philander (2000), Is El Niño changing?, *Science*, *288*, 1997–2002.

Francou, B., P. Ribstein, R. Saravia, and E. Tiriau (1995), Monthly balance and water discharge of an intertropical glacier: Zongo Glacier, Cordillera Real, Bolivia, 16°S, *J. Glaciol.*, *41*, 61–67.

Francou, B., E. Ramirez, B. Caceres, and J. Mendoza (2000), Glacier evolution in the tropical Andes during the last decades of the 20th century: Chacaltaya, Bolivia, and Antizana, Ecuador, *Ambio*, *29*, 416–422.

Francou, B., M. Vuille, P. Wagnon, J. Mendoza, and J. E. Sicart (2003), Tropical climate change recorded by a glacier in the central Andes during the last decades of the twentieth century: Chacaltaya, Bolivia, 16°S, *J. Geophys. Res.*, *108*(D5), 4154, doi:10.1029/2002JD002959.

Francou, B., M. Vuille, V. Favier, and B. Caceres (2004), New evidence for ENSO impact on low latitude glaciers: Antizana 15, Andes of Ecuador, 0°28′S, *J. Geophys. Res.*, *109*, D18106, doi:10.1029/2003JD004484.

Gaffen, D. J., B. D. Santer, J. S. Boyle, J. R. Christy, N. E. Graham, and R. J. Ross (2000), Multidecadal changes in the vertical temperature structure of the tropical troposphere, *Science*, *287*, 1242–1245.

Garreaud, R. D., and J. M. Wallace (1997), The diurnal march of convective cloudiness over the Americas, *Mon. Weather Rev.*, *125*, 3157–3171.

Greuell, W., W. Knap, and C. Smeets (1997), Elevational changes in meteorological variables along a midlatitude glacier during summer, *J. Geophys. Res.*, *102*, 25,941–25,954.

Halberstam, I., and J. P. Schieldge (1981), Anomalous behaviour of the atmospheric surface layer over a melting snowpack, *J. Appl. Meteorol.*, *20*, 255–265.

Halldin, S., and A. Lindroth (1992), Errors in net radiometry: Comparison and evaluation of six radiometer designs, *J. Atmos. Oceanic Technol.*, *9*, 762–783.

Hardy, D. R., M. Vuille, C. Braun, F. Keimig, and R. S. Bradley (1998), Annual and daily meteorological cycles at high altitude on a tropical mountain, *Bull. Am. Meteorol. Soc.*, *79*, 1899–1913.

Hastenrath, S. (1978), Heat-budget measurements on the Quelccaya Ice Cap, Peruvian Andes, *J. Glaciol.*, *20*, 85–97.

Hastenrath, S., and A. Ames (1995), Recession of Yanamarey Glacier in Cordillera Blanca, Peru, during the 20th century, *J. Glaciol.*, *41*, 191–196.

Hay, J. E., and B. B. Fitzharris (1988), A comparison of the energy-balance and bulk-aerodynamic approaches for estimating glacier melt, *J. Glaciol.*, *34*, 145–153.

Hock, R., and B. Holmgren (2005), A distributed surface energy balance model for complex topography and its application to Storglaciären, Sweden, *J. Glaciol.*, in press.

Huber, M., and R. Caballero (2003), Eocene El Niño: Evidence for robust tropical dynamics in the "hothouse", *Science*, *7*, 877–881.

Kaser, G. (1999), A review of the modern fluctuations of tropical glaciers, *Global Planet. Change*, *22*, 93–103.

Kaser, G. (2001), Glacier-climate interaction at low latitudes, *J. Glaciol.*, *47*, 195–204.

Kaser, G., and B. Noggler (1991), Observations on Speke Glacier, Ruwenzori Range, Uganda, *J. Glaciol.*, *37*, 313–318.

Kaser, G., C. Georges, and A. Ames (1996), Modern glacier fluctuations in the Huascaran-Chopicalqui massif of the Cordillera Blanca, Peru, *Z. Gletscherkd. Glazialgeol.*, *32*, 91–99.

Kimball, B. A., S. B. Idso, and J. K. Aase (1982), A model of thermal radiation from partly cloudy and overcast skies, *Water Resour. Res.*, *18*, 931–936.

Kipp and Zonen (1995), CNR1 net-radiometer instruction manual, 42 pp., Delft, Netherlands.

Kondratyev, K. (1969), *Radiation in the Atmosphere*, 1st ed., 912 pp., Elsevier, New York.

Kotlyakov, V. M., and I. M. Lebedeva (1974), Nieve and ice penitentes: The way of formation and indicative significance, *Z. Gletscherkd. Glazialgeol.*, *10*, 111–127.

Kraus, H. (1973), Energy exchange at air-ice interface, *IAHS Publ.*, *107*, 128–164.

Kuhn, M. (1978), Die Höhe des Geschwindigkeitsmaximums im Gletscherwind als Parameter des Wärmehaushalts, paper presented at Arbeiten aus der Zentralanstalt für Meteorologie und Geodynamik, Vienna, Austria.

Male, D. H., and R. J. Granger (1981), Snow surface energy exchange, *Water Resour. Res.*, *17*, 609–627.

Martin, S. (1975), Wind regimes and heat exchange on Glacier de Saint Sorlin, *J. Glaciol.*, *14*, 91–105.

Meesters, A. G. C. A., N. J. Bink, H. Vugts, F. Cannemeijer, and E. A. C. Henneken (1997), Turbulence observations above a smooth melting surface on the Greenland ice sheet, *Boundary Layer Meteorol.*, *85*, 81–110.

Mellor, M. (1977), Engineering properties of snow, *J. Glaciol.*, *19*, 15–99.

Mölg, T., C. Georges, and G. Kaser (2003), The contribution of increased incoming shortwave radiation to the retreat of the Rwenzori glaciers, East Africa, during the 20th century, *Int. J. Climatol.*, *23*, 291–303.

Moore, R. D. (1983), A comparison of the snowmelt energy budgets in two alpine basins, *Arch. Meteorol. Geophys. Bioklimatol., Ser. B*, *33*, 1–10.

Müller, H. (1985), Review paper: On the radiation budget in the Alps, *J. Climatol.*, *5*, 445–462.

Munro, D. S. (1989), Surface roughness and bulk heat transfer on a glacier: Comparison with eddy correlation, *J. Glaciol.*, *35*, 343–348.

Munro, D. S., and J. A. Davies (1978), On fitting the log-linear model to wind speed and temperature profiles over a melting glacier, *Boundary Layer Meteorol.*, *15*, 423–437.

Obled, C., and B. Rosse (1977), Mathematical models of a melting snowpack at an index plot, *J. Hydrol.*, *32*, 139–163.

Obleitner, F., and J. de Wolde (1999), On intercomparison of instruments used within the Vatnajökull glacio-meteorological experiment, *Boundary Layer Meteorol.*, *92*, 27–37.

Oerlemans, J., and B. Grisogono (2002), Glacier winds and parameterisation of the related surface heat fluxes, *Tellus, Ser. A*, *54*, 440–452.

Oerlemans, J., and W. Knap (1998), A 1 year record of global radiation and albedo in the ablation zone of Morteratschgletscher, Switzerland, *J. Glaciol.*, *44*, 231–238.

Ohmura, A. (1990), On the existence of glacier N°1, Urumqi River, in *Glacial Climate Research in the Tianshan*, edited by A. Ohmura, pp. 37–42, Geogr. Inst., Eidg. Tech. Hochsch., Zurich, Switzerland.

Olyphant, G. A. (1986), The components of incoming radiation within a mid-latitude alpine watershed during the snowmelt season, *Arct. Alp. Res.*, *18*, 163–169.

Peterson, J. A., and L. F. Peterson (1994), Ice retreat from the neoglacial maxima in the Puncak Jayakesuma, Republic of Indonesia, *Z. Gletscherkd. Glazialgeol.*, *30*, 1–9.

Platt, C. M. (1966), Some observations of the climate of Lewis Glacier, Mount Kenya, during the rainy season, *J. Glaciol.*, *6*, 267–287.

Plüss, C., and A. Ohmura (1997), Longwave radiation on snow-covered mountainous surfaces, *J. Appl. Meteorol.*, *36*, 818–824.

Prohaska, F. (1970), Distinctive bioclimatic parameters of the subtropical-tropical Andes, *Int. J. Biometeorol.*, *14*, 1–12.

Queney, P. (1974), *Elements de Météorologie*, 2nd ed., 300 pp., Masson, Paris.

Ramirez, E., B. Francou, P. Ribstein, M. Descloîtres, R. Guérin, J. Mendoza, R. Gallaire, B. Pouyaud, and E. Jordan (2001), Small-sized glaciers disappearing in the tropical Andes: A case study in Bolivia—The Chacaltaya Glacier, 16°S, *J. Glaciol.*, *47*, 187–194.

Ribstein, P., E. Tiriau, B. Francou, and R. Saravia (1995), Tropical climate and glacier hydrology: A case study in Bolivia, *J. Hydrol.*, *165*, 221–234.

Schwerdtfeger, P. (1976), *Physical Principles of Micrometeorological Measurements*, 1st ed., 111 pp., Elsevier, New York.

Seltzer, G. O. (2001), Late Quartenary glaciation in the tropics: Future research directions, *Quat. Sci. Rev.*, *20*, 1063–1066.

Sicart, J. E., P. Ribstein, P. Wagnon, and D. Brunstein (2001), Clear sky albedo measurements on a sloping glacier surface: A case study in the Bolivian Andes, *J. Geophys. Res.*, *106*, 31,729–31,738.

Sicart, J. E., P. Ribstein, J. P. Chazarin, and E. Berthier (2002), Solid precipitation on a tropical glacier in Bolivia measured with an ultrasonic depth gauge, *Water Resour. Res.*, *38*(10), 1189, doi:10.1029/2002WR001402.

Sicart, J. E., P. Ribstein, B. Francou, and R. Gallaire (2003), Etude des précipitations et de la fonte sur un glacier tropical: Le glacier du Zongo, Bolivie, 16S, *Hydrol. Sci. J.*, *48*, 799–808.

Sicart, J. E., P. Ribstein, B. Francou, B. Pouyaud, and T. Condom (2005), Glacier mass balance of tropical Zongo glacier, Bolivia, comparing hydrological and glaciological methods, *Global Planet. Change*, in press.

Smeets, C., P. Duynkerke, and H. Vugts (1998), Turbulence characteristics of the stable boundary layer over a mid-latitude glacier, part I: A combination of katabatic and large-scale forcing, *Boundary Layer Meteorol.*, *87*, 117–145.

Thompson, L. G. (2000), Ice core evidence for climate change in the tropics: Implications for our future, *Quat. Sci. Rev.*, *19*, 19–35.

Trenberth, K. E., and T. J. Hoar (1996), The 1990–1995 El Niño–Southern Oscillation event: Longest on record, *Geophys. Res. Lett.*, *23*, 57–60.

Van den Broeke, M. (1997), Momentum, heat and moisture budgets of the katabatic wind layer over a midlatitude glacier in summer, *J. Appl. Meteorol.*, *36*, 763–774.

Van den Broeke, M., C. H. Reijmer, and R. S. W. Van de Wal (2004), Surface radiation balance in Antarctica as measured with automatic weather stations, *J. Geophys. Res.*, *109*, D09103, doi:10.1029/2003JD004394.

Van der Avoird, E., and P. G. Duynkerke (1999), Turbulence in a katabatic flow, *Boundary Layer Meteorol.*, *92*, 39–66.

Visser, K., R. Thunell, and L. Stott (2003), Magnitude and timing of temperature change in the Indo-Pacific warm pool during deglaciation, *Nature*, *421*, 152–155.

Vuille, M., R. S. Bradley, and F. Keimig (2000), Interannual climate variability in the Central Andes and its relation to tropical Pacific and Atlantic forcing, *J. Geophys. Res.*, *105*, 12,447–12,460.

Vuille, M., R. S. Bradley, M. Werner, and F. Kleimig (2003), 20th century climate change in the tropical Andes: Observations and model results, *Clim. Change*, *59*, 75–99.

Wagnon, P., P. Ribstein, B. Francou, and B. Pouyaud (1999), Annual cycle of energy balance of Zongo Glacier, Cordillera Real, Bolivia, *J. Geophys. Res.*, *104*, 3907–3923.

Wagnon, P., P. Ribstein, B. Francou, and J. E. Sicart (2001), Anomalous heat and mass budget of Glaciar Zongo, Bolivia, during the 1997/98 El Nino year, *J. Glaciol.*, *47*, 21–28.

Wagnon, P., J. E. Sicart, E. Berthier, and J. P. Chazarin (2003), Wintertime high-altitude surface energy balance of a Bolivian glacier, Illimani, 6340 m above sea level, *J. Geophys. Res.*, *108*(D6), 4177, doi:10.1029/2002JD002088.

Webb, E. K. (1970), Profile relationships: The log-linear range, and extension to strong stability, *Q. J. R. Meteorol. Soc.*, *96*, 67–90.

Wielicki, B. A., T. Wong, and R. P. Allan (2002), Evidence for large decadal variability in the tropical mean radiative energy budget, *Science*, *295*, 841–844.

Zuo, Z., and J. Oerlemans (1996), Modelling albedo and specific balance of the Greenland ice sheet: Calculations for the Søndre Strømfjord transect, *J. Glaciol.*, *42*, 305–317.

J. E. Sicart, Great Ice–IRD, Université Montpellier II, 300, Avenue du Professeur Emile Jeanbrau, F-34095 Montpellier Cedex 5, France. (sicart@msem.univ-montp2.fr)

P. Wagnon, Great Ice–IRD, LGGE, 54 Rue Molière, BP96, F-38402, Saint Martin d'Hères Cedex, France.

P. Ribstein, UMR Sisyphe, UPMC, case 123, 4 Place Jussieu, F-75252 Paris Cedex 05, France.